Sensors and Materials, Vol. 36, No. 12 (2024) 5507–5520
MYU Tokyo

S & M 3882

Improved Delaunay-triangulation-based 3D Geological Modelling Algorithm for Power Pylons

JingGuo Lv,[1*] BangZheng He,[1] HongBo Wu,[2]
JiYong Zhang,[2] ChunHui Zhao,[2] and JunJie Sun[3]

[1]College of Surveying and Urban Spatial Information, Beijing University of Civil Engineering and Architecture, Beijing 102616, China
[2]State Grid Economic and Technical Research Institute Co., Beijing 102200, China
[3]Economic Research Institute of State Grid ZheJiang Electric Power Company, Hangzhou 310020, China

(Received August 29, 2024; accepted December 6, 2024)

Keywords: 3D geological model, grid towers, Delaunay triangulation, Kriging interpolation

To construct an accurate 3D geological model of the grid engineering tower scene, we propose a method for 3D geological modelling of grid engineering towers on the basis of borehole data. The method generates a more accurate 3D geological model by improving the Delaunay triangulation algorithm and combining it with Kriging interpolation to process the borehole data. Furthermore, a detailed adjustment of the model is achieved through the introduction of geological profiles. The 3D geological model is constructed using the operational area of the power grid engineering survey as a case study, thereby accurately reflecting the geological conditions of the region. The results of testing demonstrate that the modelling method in this paper is more accurate than existing methods, and the generated 3D geological model not only provides a scientific foundation for tower placement and line design but also offers valuable insights for advancing the digital transformation of power grid engineering.

1. Introduction

As a consequence of the accelerated development of power grid projects, particularly those of an ultrahigh-voltage (UHV) nature, the number and distribution of towers in such projects are increasing while the geological conditions to which they are subject are becoming increasingly complex. 3D geological modelling is a process that employs spatial data to construct a geometric model reflecting the spatial location, geometry and spatial relationship of underground geological interfaces and geological bodies, including strata and faults. A 3D geological model allows power grid engineering geologists to accurately assess geological conditions and identify geologically stable areas. This enables designers to avoid high-risk areas where landslides, subsidence, and other geological hazards are more likely to occur in tower siting and thus, to form the most optimal line selection scheme.

In recent years, scholars at home and abroad have conducted comprehensive research on 3D geological modelling methods. Liang *et al.*(1) employed the Markov chain Monte Carlo method

*Corresponding author: e-mail: lvjingguo@bucea.edu.cn
https://doi.org/10.18494/SAM5352

ISSN 0914-4935

(MCMC) to develop multilayer geological models. Wu *et al.*[2] integrated cross-sectional and profile data to propose a 2D–3D linkage approach for the 3D geological modelling of regional cross sections. Song and Tsai[3] introduced the interval Kriging method, which utilizes binary indexes for lithology modelling and visualization based on 3D boreholes. Wang *et al.*[4] constructed a 3D geological model using the irregular triangular mesh-generalized trigonal prism (TIN-GTP) algorithm, utilizing borehole data to construct geological models at varying scales. Hou *et al.*[5] conducted 3D geological modelling and visualization based on the Dassault 3DE platform. Nevertheless, the lack of sufficient raw data represents a significant obstacle to the accurate establishment of 3D geological models.

In a series of studies, scholars have employed borehole data to extract information about the geological properties of the subsurface and to construct 3D geological models. Lv *et al.*[6] created a 3D model by extracting and processing vectorized information from remotely sensed geological interpretation maps and combining it with drill-hole data. Similarly, Xu *et al.*[7] used multisource data to establish a 3D geological solid model integrating the surface, tectonics, ore bodies, and stratigraphy. For the problem of large intervals between neighboring drill-hole data, Sun *et al.*[8] proposed the theory and method of interpolation smoothing for the three-prism 3D geological model. Feng *et al.*[9] employed the boosting integration strategy to construct a 3D geological model based on gas extraction borehole data. Tseng *et al.*[10] proposed a numerical framework to integrate multisource data and construct a 3D geological model in a multifidelity prediction model. Cole *et al.*[11] combined geological mapping and borehole and seismic reflection data to construct a 3D geological model. The aforementioned methods enhance the explanatory power and prediction accuracy of the data by employing the principles of geostatistics, machine learning algorithms, and multisource data. However, further research is required to develop a comprehensive and accurate 3D geological model.

At present, 3D geological modelling algorithms have been the subject of extensive study in a number of fields, including petroleum exploration, oilfield development, and mineral resources development. However, in the context of grid engineering towers, the focus has been primarily on the modelling algorithms associated with the tower structure itself. Additionally, there has been relatively limited research conducted on underground geological modelling algorithms. Consequently, the tower scene of the underground space situation in a three-dimensional model has not been sufficiently explored to achieve effective visualization.

Therefore, through the improvement of the Delaunay triangular sectioning algorithm, the combination with Kriging interpolation to process the borehole data, and the introduction of the optimal modelling method of profile correction, we established a 3D geological model of power grid pole tower by taking the actual operation area of a power grid engineering survey business as an example. By visualizing and analyzing the geological condition of the area, important guidance is gained for designing the site selection of the pole tower.

2. Related Theory

2.1 Delaunay triangulation algorithm

Delaunay triangulation (DT) represents a foundational concept in the field of computational geometry, and it serves as a crucial preparatory technique across a range of disciplines, including numerical analysis, information visualization, and computer graphics. In 1934, the Russian mathematician B. Delaunay proposed DT, which is a set of Voronoi diagrams with a rigorous mathematical definition and comprehensive theoretical foundation. The Delaunay triangular mesh is regarded as the optimal triangular mesh owing to its superior geometrical properties, including the empty outer circle and the maximum of the smallest angle, among others. It is employed in a number of fields, including geographic information systems, computer simulation, geology, computer graphics, and virtual reality. The triangular mesh possesses the properties of null circularity and maximization of the minimum angle, as shown in Fig. 1.

Empty circularity: The Delaunay triangular network is unique in that no four points can be cocircular. Furthermore, no other points can exist inside any of the triangles in that network.

Maximizing of the minimum angle: The minimum angle of a triangle generated by a Delaunay triangular network is the largest among the triangular networks that may be formed by the scatter set generated by the projection of the observation set. This is known as the 'minimum angle' and it can be increased by optimizing the network.

Let us assume that there exists a finite point set V defined in R^n space. Then, M is a convex packet of the point set V, T is a triangular network of the convex packet M, and $f_{I,T}$ denotes the segmented linear finite element interpolation of a continuous convex function f defined on M. In this case, the error-based mesh quality defined by the Minkowski distance is given by the following expression.

$$Q(T, f, p) = \left(\int_M | f(x) - f_{I,T}(x) |^P dx\right)^{\frac{1}{P}} \tag{1}$$

Equation (1) is used to quantify the quality of a finite set of points in a mesh. Smaller values of the equation represent a higher quality of the mesh, which is optimal when the triangular network T^* satisfies

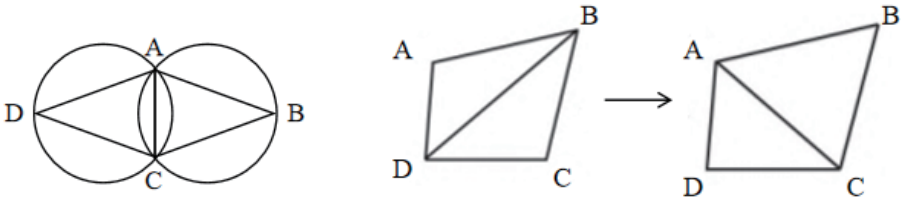

(a) (b)

Fig. 1. Two conditions for DT: (a) empty circularity and (b) maximizing of the minimum angle.

$$Q(T^*, f, p) = \inf Q(T, f, p). \tag{2}$$

2.2 DT algorithm

Kriging interpolation is a type of interpolation method that is used to calculate the value of unknown points using the known point values. It is a widely used method in a number of fields, including terrain data reconstruction, precipitation prediction, and geological and mineral exploration, because it is a linear, optimal estimation, and unbiased method.[12,13] The fundamental principle of Kriging interpolation is a semivariational function theory, which is employed to elucidate the transformation of spatial random variables in response to changes in spatial location, as well as to demonstrate a decline in these variables with an increase in distance. The semivariational function is expressed as follows.

$$\gamma_{i,j} = \frac{1}{2} D(Z_i - Z_j) = \sigma^2 - Cov(Z_i, Z_j) \tag{3}$$

In Eq. (3), $D(Z_i, Z_j)$ represents the variance of the difference between the measurements at the i and j measurement points. Equation (3) is consistent with the following assumption: the variance of each measurement point in the region is σ^2. On this basis, the semivariance function $\gamma_{i,j}$ can be related to the covariance $Cov(Z_i, Z_j)$ between the two measurements Z_i and Z_j. The covariance $Cov(Z_i, Z_j)$ is typically solved approximately on the basis of the grouping of the steps, with the discrete semivariance function values calculated using the known values. The fitted model is then used to fit the semivariance function values at different distances employing commonly used models such as the spherical, exponential, and Gaussian models.[14] The interpolated value of an unknown point is the weighted sum of the known values in its vicinity. To ensure the unbiased nature of the interpolated value, the following relation is established.

$$E(\sum_{i=1}^{n} \lambda_i Z_i) = E(Z_0) \tag{4}$$

In this equation, λ_i represents the weight corresponding to each Z_i, Z_0 denotes the value of the unknown point, and Z_i signifies the value of the i point among the known n points. When Eq. (4) satisfies the implicit smoothness assumption, the following can be derived.

$$\sum_{i=1}^{n} \lambda_i = 1 \tag{5}$$

Equation (5) indicates that the sum of all the weights is 1. From this, the optimal estimator qualification is established, and the variance of the difference between the unknown point estimate and its true value is minimized, which is expressed as

$$D(\sum_{i=1}^{N}\lambda_i Z_i - Z_0) = \min . \tag{6}$$

Equations (3), (5), and (6) can be combined to obtain an expression for the weights λ and the semivariance function γ that attains a minimum value.

$$2\sum_{i=1}^{n}\lambda_i\gamma_{r,0} - \gamma_{i,0} - \sum_{i=1}^{n}\sum_{j=1}^{n}\lambda_i\lambda_j\gamma_{r,j} = \min \tag{7}$$

Equations (5) and (7) constitute the conditional extreme value problem, whereby the known point weights in the vicinity of the unknown point are solved by the Lagrange multiplier method. The value obtained by Kriging interpolation of the unknown point is the weighted sum of the values in its vicinity, that is to say, the Kriging interpolated value of the unknown point Z_0 is $\sum_{i=1}^{n}\lambda_i Z_i$.

3. Algorithm for 3D Geological Modelling of Power Grid Towers

The 3D geological modelling algorithm proposed in this paper consists of three stages: data processing, data interpolation, and model modification. The algorithm flow is shown in Fig. 2.

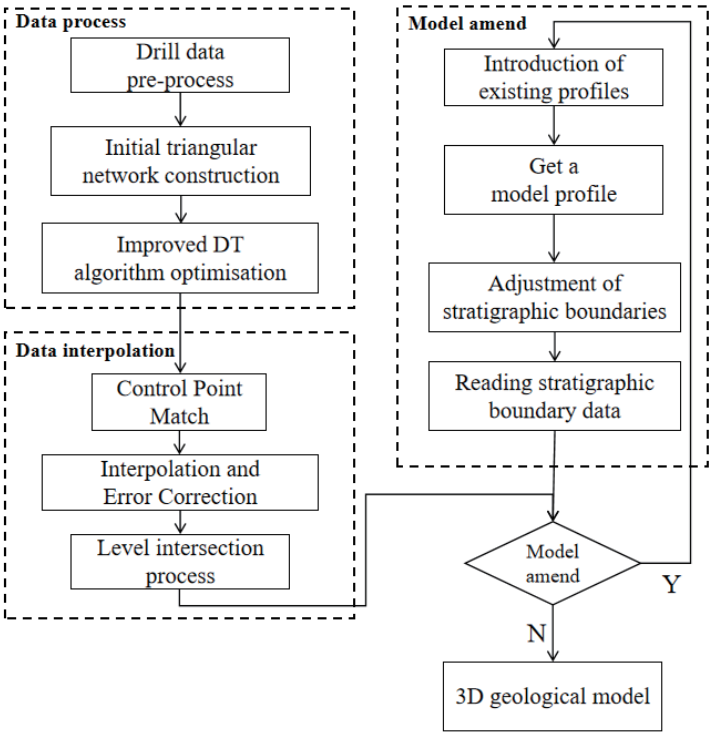

Fig. 2. Algorithm flow of 3D geological modelling.

3.1 Borehole data processing using improved DT algorithm

The power grid engineering tower scene is typified by intricate topographical features, a substantial data volume, and inaccuracies in the data, which will result in the original DT algorithm encountering challenges such as diminished efficiency, limited adaptability to complex terrain, and the generation of superfluous imaginary triangles when dealing with large-scale data.[15–17] To address the above problems, we chose the Bowyer–Watson algorithm as the basis for improving the Delaunay triangular network algorithm. The basic idea is that the initially generated triangular network is first optimized to avoid generating overlapping, crossing or imaginary triangles and to ensure that all data points are included. Then the point-set-by-point insertion process is optimized to improve the search efficiency and to quickly locate the neighbors of the new points. Finally, irregularities in the edges of the triangular mesh are corrected to ensure that there are no overlapping or crossing triangles and that no other data points are included in the outer circles of the triangles.

The improved DT algorithm consists of three parts: expanding the initial supertriangles, point-by-point insertion optimization based on $O(n)$-order search trees, and convex packet detection.

3.1.1 Expanding the initial supertriangle

The Bowyer–Watson algorithm commences with the construction of a triangle (supertriangle) of sufficient magnitude to encompass all the points in question. As the algorithm progresses and new points are inserted, it may be necessary to remove the sides of the supertriangle that intersect those points. This process involves more complex calculations, which will affect the efficiency of the algorithm.

A common method is the similar triangle theorem construction; however, this is insufficient for the inclusion of all points, necessitating an additional expansion of the triangle. To address this issue, the construction of imaginary triangles is circumvented by a reexpansion of the initial supertriangle. In other words, a supertriangle is constructed on the basis of the maximum distribution of discrete points with the objective of encompassing all the points in set X.

3.1.2 Point-by-point insertion optimization based on $O(n)$-order search trees

In the Bowyer–Watson algorithm, the process of inserting a new point necessitates the identification of an appropriate position within the existing triangular mesh. This typically necessitates a search of the point set to ascertain the relationship between the new point and the existing triangles, as well as the necessary updates to the triangular mesh. The process requires the point set to be sorted in order to optimize the search and insertion operations, particularly when the point set is large. The sorting and search operations can consume a significant amount of computational resources.

To enhance efficiency, we employed a point-by-point insertion methodology founded upon an $O(n)$-order search tree for optimization. The fundamental concept underlying the methodology is that of neighbor alignment and hierarchical joining. The specific steps involved are as follows.

(1) Adjacency arrangement: First, on the basis of the *x*-coordinates of the points, the point set is sorted using a fast sorting algorithm to ensure that each point is stored in the array in the given order. A balanced binary search tree is constructed using the sorted point set, and when a new point needs to be inserted, its structure can be quickly located to where the new point should be inserted. When inserting a new point using the nature of a binary search tree, one can quickly locate its neighboring points, thus reducing the search range.
(2) Hierarchical joining: The point set X is divided into multiple levels, with each level $X(i)$ exhibiting a certain degree of uniformity in different distributions. Consequently, when inserting new points, the search can be prioritized within the same level or adjacent levels, thus enhancing the efficiency of the search process.
(3) Optimization of insertion: The aforementioned arrangement and grading facilitate the expedient insertion of new points into the correct position while maintaining the Delaunay nature of the triangular mesh.

3.1.3 Convex packet detection

During the construction of Delaunay triangular meshes, irregularities may be formed at the edges of the triangular mesh, particularly in the case of point-by-point insertion. Furthermore, if the points are inserted in an inappropriate sequence, it is possible to generate imaginary triangles that do not intersect with the convex hulls of the point set. To address these issues, we employ convex packet detection to assist in the identification of irregularities and facilitate necessary adjustments.

The initial step is the introduction of vector fork multiplication, as illustrated in Fig. 3. Two line segments are deemed to intersect if the conditions set forth in Eq. (8) are met; otherwise, they are considered to be nonintersecting.

$$(CA \times CD) \times (CB \times CD) \leq 0 \tag{8}$$

Accordingly, the generated edge points are employed to construct a line segment connecting each point in a specific geometric sequence. In the event that this line segment does not intersect with a line segment within the triangular network that has already been generated, it is constituted as an edge segment between the aforementioned points. The newly formed triangles are then incorporated into the triangular network.

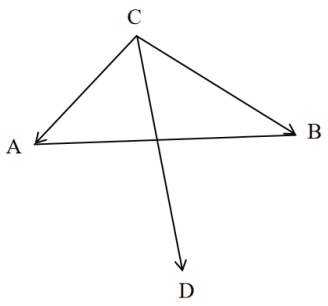

Fig. 3. Schematic of vector cross product.

3.2 Data interpolation and replacement

To guarantee the continuity and uniformity of the levels throughout the process of geological level interpolation, it is essential to align the data with control points. Typically, the points to be interpolated are identified by spatial regions situated between existing borehole data points. The original borehole points are imported into the scatterplot as control points, and for each control point, the interpolation point with the closest distance is identified. Subsequently, Kriging interpolation was employed to generate preliminary geological level *Z*-values. In instances where the level *Z* value of the interpolated point differs significantly from that of the control point, we employ a data error reduction strategy whereby the level *Z* value of the interpolated point is replaced with the actual level elevation of the control point.

The interpolated stratigraphic data will exhibit the phenomenon of the intersection of levels, whereby the elevation of the lowest points in the previous soil layer is lower than the elevation of the corresponding points in the soil layer below it. In this study, the elevation of the bottom of a specific soil layer is compared with the elevation of the subsequent soil layer, from the top to the bottom. When the elevation value Z_i of a given point on the current soil layer is less than the elevation value Z_{i+1} of the corresponding point on the soil layer below it, the elevation value Z_{i+1} of the bottom of the next soil layer is replaced by the elevation value Z_i of the points on the current soil layer, thus ensuring greater clarity in the delineation of the layers.

3.3 Profile model amendment

The utilization of borehole data for the direct establishment of the model is a relatively straightforward and commonly employed methodology. However, the exclusive reliance on borehole data modelling frequently proves inadequate for achieving an accurate correspondence with the actual geological circumstances. At this juncture, the integration of a cross section of the model with amendments serves to enhance the model's conformity with the authentic stratigraphic trajectory of the geological landscape, thereby approximating the actual geological situation.

In accordance with the tenets of spatial data comparison, we employed a comparative approach to examine the discrepancies between the stratigraphic distribution observed on the geological profile and that depicted in the 3D geological model.[18] The corresponding profiles were extracted from the 3D geological model by means of a cutting operation conducted along a specific direction within the model. A comparison of the extracted profiles with the geological profile will allow for the identification of any discrepancies in the model.

A comparison of the stratigraphic demarcation lines in the model profile with those in the geological profile allows for the modification of any discrepancies between the two, including the offset of the stratigraphic position, the presence of missing or redundant strata in the model, and any other inconsistencies. This ensures that the stratigraphic demarcation line in the model aligns with the actual geological situation. In this paper, we put forth a methodology for adjusting ground demarcation lines using the principle of least squares. In the method, the weighted least squares approach is employed to achieve the optimal adjustment of height values.

The weights are determined in accordance with the distance between the points and the corresponding points in the geological profile, thereby enhancing the effect of the nearest-neighbor data. The model prediction error is then iteratively solved to achieve its minimization. The calculation equation is as follows.

$$Z_{\mathrm{i}}^{'} = \frac{\sum_{j}^{i} w_j Z_j}{\sum_{j}^{i} w_j} \tag{9}$$

$$w_j = \left(\frac{1}{d_{i,j}} \right)^2 \tag{10}$$

In these equations, $Z_i^{'}$ represents the adjusted height value of the i point, Z_j denotes the height in the geological profile in the vicinity of point $\mathrm{p_i}$, and w_j is the weight calculated from the distance $d_{i,j}$ between points $\mathrm{p_i}$ and Z_j.

3.4 Profile model amendment

To ascertain the veracity of the modelling method, the constructed model must be validated. In this study, the accuracy of specific elevation points was employed as a means of testing the model, namely, to ascertain whether the stratigraphic elevation data of the model are consistent with the actual data at a given coordinate position. To construct a 3D geological model using the conventional method as described in the literature, some original borehole data are reserved beforehand.[19] The remaining drill holes were employed as modelling data to be used in the aforementioned processing of drill-hole data, which encompasses the improved DT algorithm, data interpolation and replacement, and profile model correction processing, with the objective of constructing a 3D geological model. The results obtained with the optimized model were read in accordance with the *XY* coordinates of the validation sample points in order to obtain the elevation of each level. The model accuracy was validated by comparing the model results with the validation samples, using the two assessment indexes of mean absolute error (*MAE*) and root mean square error (*RMSE*), as outlined in Ref. 20. The equations are as follows.

$$MAE = \frac{1}{n} \sum_{i=1}^{n} | M_i - O_i | \tag{11}$$

$$RMSE = \sqrt{\frac{1}{n} \sum_{i=1}^{n} (M_i - O_i)^2} \tag{12}$$

In this equation, the variable n represents the number of stratigraphic levels, M_i denotes the model data, and O_i signifies the raw data.

4. Experiment

4.1 Data source

The bore-hole data from the third operation area of Section 2-1 of the Ningxia–Hunan ±800 kV UHV DC transmission line were subjected to 3D geological modelling and analysis experiments, employing the methodology outlined in this paper. The operation area is characterized by crustal subsidence since the Quaternary, which has resulted in the formation of extensive alluvial and lacustrine plain landscapes. The Quaternary stratigraphy is widely distributed and thick, comprising primarily Holocene sediments, Late Pleistocene alluvial and lacustrine sediments, and interbedded land and sea sediments. In accordance with the data obtained from the exploration, the engineering geological layers can be classified into ten distinct categories, arranged from the topmost layer to the bottommost layer and from the most recent to the earliest formation. The soil layers are as follows: (1) silt soil layer, (2) loess layer, (3) sand soil layer, (4) clay layer, (5) brown soil layer, (6) organic soil layer, (7) grey cover soil layer, (8) powdery clay layer, (9) powdery soil layer, and (10) powdery clay layer. A total of 142 bore holes were drilled within the operation area, 106 of which are currently available and have been numbered Z1–Z106.

4.2 Data model

The five original drill holes, designated Z15, Z35, Z55, Z75, and Z95, were reserved as validation samples, while the remaining 101 drill-hole point data were employed in the construction of the 3D geological model using the methodology proposed in this paper. Prior to interpolation, the boundaries in the X and Y directions were defined in accordance with the

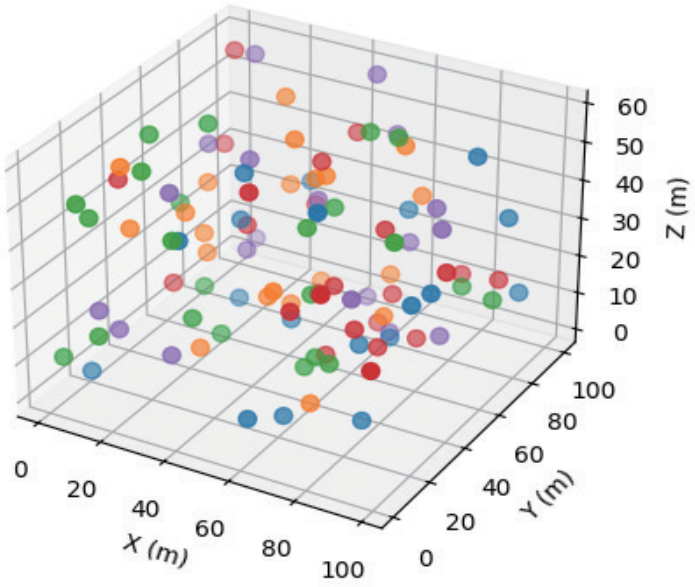

Fig. 4. (Color online) Distribution of drill-hole locations in the work area.

extent of the study area. The original borehole points were employed as control points, and the scatter plots generated by the enhanced DT algorithm and the data interpolated by Kriging interpolation were utilized to identify the nearest interpolation point to each control point. This was followed by the analysis of the discrepancy between the control point and the interpolation point corresponding to the elevation of each level and the acquisition of the frequency statistics of the absolute value interval of the error, as illustrated in Table 1. The overall accuracy of the interpolated data is high. However, there are some instances where the interpolated data deviate significantly from the actual data. In such cases, the Z value of the corresponding interpolated point with an absolute error greater than 0.6 in each level is replaced with the corresponding level elevation of the control point, thus ensuring greater accuracy.

Subsequently, the intersection of the layers is processed to obtain the XYZ data of each layer, which serve as the foundation for the generation of the stratigraphic triangulation mesh surface domain. The triangular mesh surfaces are created in a sequential manner, with interpolated points appended to each surface to construct the 3D geological model. In the event of a discrepancy between the model-generated profiles and the profiles of the existing geological data pertaining to the stratigraphic boundaries, the model is duly corrected through the redrawing of said boundaries by the ground boundary adjustment method, which is based on the principle of least squares. Figure 5 depicts the final model.

4.3 Model validation

The reserved boreholes Z15, Z35, Z55, Z75, and Z95 were selected for analysis. The sample data were then compared with the model data, and the resulting errors were calculated using the validation Eqs. (11) and (12). The results are presented in Table 2. The discrepancy between the model constructed using the methodology presented in this paper and the sample model is

Table 1
Absolute error absolute value interval and frequency.

Absolute error absolute value interval	[0, 0.3)	[0.3, 0.6)	[0.6, 1.0)	[1.0, +∞)
Frequency	452	207	32	8

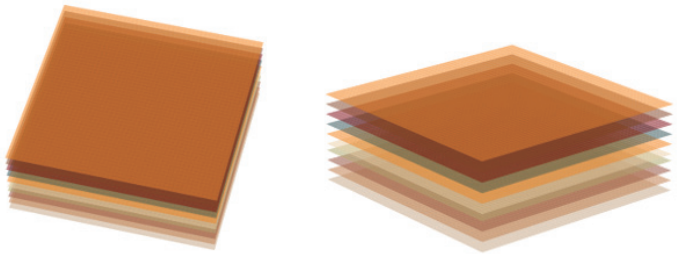

(a) (b)

Fig. 5. (Color online) 3D geological model of the working area and layering. (a) 3D geological model. (b) Model layered display.

Table 2
Model accuracy validation. (Unit: m)

Drill hole number	Shared data access control large-scale dataset		Permission update proxy reencryption	
	Sample model	Our	Sample model	Our
Z15	0.532	0.259	0.568	0.116
Z35	0.473	0.198	0.487	0.157
Z55	0.837	0.705	0.902	0.424
Z75	0.764	0.437	0.821	0.382
Z95	1.246	0.921	1.268	0.517

evident, with the former exhibiting markedly reduced *MAE* and *RMSE* values. These values are lower than those observed in the sample model by 0.132 to 0.327 m and 0.33 to 0.751 m, respectively. Consequently, the modelling approach proposed in this paper is capable of effectively optimizing the model, enhancing its accuracy, and facilitating the establishment of a more realistic and reliable 3D geological model.

5. Conclusions

A 3D geological modelling method for power grid towers based on borehole data was proposed in this paper. A 3D geological model of the third operation area of Section 2-1 of the Ningxia–Hunan ±800 kV UHV DC transmission line was established as an example to confirm the reliability of the modelling method. By improving the Delaunay triangular sectioning algorithm, combining it with Kriging interpolation to deal with the drilling data, and introducing profile correction, a more accurate 3D geological model was generated, which was able to satisfy the requirements of the 3D geological model for the geological exploration of the grid project tower scene with higher quality. Through the visualization of the geological 3D model, the undulation and change rule of the strata in the study area were shown clearly and intuitively, and the 3D model could be cut flat to understand the distribution of soil layers at different depths, which, combined with the physical and mechanical properties of the soil layers in the survey data, helped to judge the geological situation near the tower and within different depths.

In the future, research is planned to further improve the generality of this method and realize integration research with numerical simulation. At the same time, for some tower survey areas, it is also planned to combine the data collected by UAVs, satellite image data, and DEM data to carry out fusion research and realize more accurate 3D geological modelling.

Acknowledgments

This study was supported by the Science and Technology Project of the State Grid Corporation of China: Research and Application of Multi-source Collaborative and Dynamic Data Sharing Technology for Power Grid Engineering Survey Data (5700-202356317A- 1-1-ZN).

References

1 Z. Liang, F. Wellmann, and O. Ghattas: Geophysics **88** (2023) 1. https://doi.org/10.1190/geo2021-0728.1
2 X. Wu, G. Liu, W. Fan, S. Peng, G. Chen, J. Cheng, and Y. Wu: Earth Sci. Inf. **17** (2024) 1067. https://doi.org/10.1007/S12145-024-01221-W
3 Y. Song, F. Tsai: Water Resour. Res. **60** (2024) 035020. https://doi.org/10.1029/2023WR035020
4 X. Wang, Z. Liu, D. Zhang, L. Ma, B. Chen, X. Lei, B. Bai, and J. Yan: Coal Geol. Explor. **41** (2024) 52. https://doi.org/10.12363/issn.1001-1986.24.04.0222
5 B. Hou, J. Xu, and B. Zhang: Yangtze River. **55** (2024) 241. https://doi.org/10.16232/j.cnki.1001-4179.2024.S1.050
6 X. Lv, J. Bai, J. Zhuang, L. Nie, and C. Gao: J. China Railway Soc. **46** (2024) 105. https://doi.org/10.3969/j.issn.1001-8360.2024.02.012
7 J. Xu, D. Xue, and Y Li: Geol. Bull. China **42** (2023) 1203. https://doi.org/10.12097/j.issn.1671-2552.2023.07.011
8 L. Sun, Y. Liu, R. Zhang, Y. Yang, and J. Yan: Chin. J. Geotech. Eng. **45** (2023) 244. https://doi.org/10.11779/CJGE2023S10049
9 Y. Feng, G. Wen, J. Shang, S. Wen, and B. Wu: Ore Geol. Rev. **171** (2024) 106157. https://doi.org/10.1016/j.oregeorev.2024.106157
10 C. Tseng, M. Ghadiri, P. Kumar, and H. Meidani: Adv. Water Resour. **178** (2023) 104486. https://doi.org/10.1016/j.advwatres.2023.104489
11 J. Cole, C. Finn, and S. Webb: Precambrian Res. **259** (2021) 106219. https://doi.org/10.1016/j.precamres.2021.106219
12 H. Wan, H. Qi, and S. Shang: Trans. Chin. Soc. Agric. Mach. **54** (2023) 339. https://doi.org/10.6041/j.issn.1000-1298.2023.01.034
13 Q. Wang, W. Ding, Z. Zhao, A. Li, and Y. Qiao: China Civil Eng. J. **55** (2022) 66. https://doi.org/10.15951/j.tmgcxb.2022.s2.04
14 S. Wang, and Y. Zhu: Met. Mine. **11** (2019) 142. https://doi.org/10.19614/j.cnki.jsks.201911024
15 X. Wu, S. Wang, and C. Xiao: Acta Geodaetica et Cartographica Sinica **01** (1999) 30. https://doi.org/10.3321/j.issn:1001-1595.1999.01.006
16 X. Zhou, and Y. Li: Comput. Eng. Appl. **49** (2013) 198. https://doi.org10.3778/j.issn.1002-8331.1108-0137
17 S. Rebay: J. Comput. Phys. **106** (1993) 125. https://doi.org/10.1006/jcph.1993.1097
18 B. Wen, J. He, Z. Chen, X. Li, and C. Jia: Surv. Mapp. **03** (2016) 118. https://doi.org/10.13474/j.cnki.11-2246.2016.0102
19 M. Yu, J. Wu, Y. Wang, W. Shi, and X. Wang: J. Disaster Prev. Mitig. **43** (2023) 588. https://doi.org/10.13409/j.cnki.jdpme.20210815002
20 W. Scott, C. Covell, E. Júlíusson, A. Valfells, J. Newson, B. Hrafnkelsson, H. Pálsson, and M. Gudjónsdóttir: Geotherm. Energy **7** (2019) 1. https://doi.org/10.1186/s40517-019-0143-6

About the Authors

Bangzheng He received his B.S. degree from Lanzhou University of Technology, China, in 2023 and has been studying at Beijing University of Civil Engineering and Architecture, majoring in photogrammetry and remote sensing. His interests are in remote sensing intelligent interpretation, remote sensing data processing, and multisource sensors and their applications in the Internet of Things.

Jingguo Lv received his Ph.D. degree in charting and geographic information science from Beijing Normal University in 2009. Since 2009, he has been teaching at Beijing University of Civil Engineering and Architecture, where he is currently an associate professor. His research interests include remote sensing information extraction, digital image processing, and visual tracking. He has published more than 40 related articles, published four academic monographs, and authored seven invention patents. He has been awarded nine software copyrights and several technological awards.

Jiyong Zhang received his B.S. degree from Wuhan University, China, in 2000. He is currently a Senior Expert and a Senior Chief Engineer at the State Grid Economic and Technical Research Institute Co., Ltd. His research directions include the study of electric power remote sensing technology, electric power data processing, and the construction of data standard systems. He has undertaken and completed multiple national, industry, and state grid company scientific research projects in these fields.